Chapter 6

Deposition of Pt on the Cu(100) surface

6.1 Introduction

Alloys and bimetallic surfaces have received much attention in recent years due to their importance in many modern technological processes (e.g. heterogeneous catalysis and magnetic recording [7, 166, 167]). As discussed in chapter 2, under certain circumstances the deposition of one metal on to a substrate of a second metallic species (e.g. Pt on Cu(100)), allows the production of surface alloys with controllable concentrations and may present surfaces with different characteristics to those of single crystal bulk alloys (e.g. $Cu_xPt_y(100)$). Such surfaces may well offer interesting electronic or chemical properties which may be of use in modern industry.

The Cu-Pt surface alloy system has been the subject of numerous studies, ranging from Cu deposition on Pt surfaces [168–171], to the surfaces of single crystal bulk alloys [172, 173] and Pt deposition on Cu surfaces. The formation of CuPt alloys on the Cu(111) surface by deposition and subsequent annealing of Pt has also been studied using many experimental and theoretical techniques [56, 174–179]. These studies have shown the room temperature formation of a Pt thin film on top of the Cu(111) surface, which diffused into the bulk Cu on annealing at around 300°C. A post-annealing alloy with a composition of approximately Cu_3Pt in the outermost layers was observed in most cases. However, Dastor *et al.* have recently shown the formation of an alloy following low temperature Pt deposition, prior to the formation of the Cu_3Pt post-annealing alloy [180].

Similar studies of Pt deposition on the Cu(100) surface have been both less common and less conclusive than on the (111) surface. Graham *et al.* were one of the first to publish data on the Pt/Cu(100) system [181]. AES, LEED and LEIS were used to suggest that Pt formed disordered islands on the surface during room temperature Pt deposition. Some intermixing with the surface layer of the Cu substrate was also

observed, along with a weak c(2×2) LEED pattern. The LEED pattern improved markedly upon annealing to 300°C. The ordering was attributed to the formation of a purely Cu surface layer, with a Cu-Pt alloy below the surface.

This view is shared by Al Shamaileh *et al.* after they investigated the system using TLEED [182]. Post-annealing analysis revealed the formation of a pure Cu surface layer at Pt coverages of 0.5 ML, 1.0 ML and 1.5 ML. Below the surface, alternating layers of purely Cu and a PtCu alloy were reported at Pt coverages of 1.0 ML and 1.5 ML. Reilly *et al.* also observed a poorly ordered c(2×2) reconstruction after room temperature Pt deposition [183]. Again, the formation of a pure Cu surface layer and a sub-surface alloy was reported following annealing, this time at 230°C.

Belkhou *et al.* deposited Pt at higher coverages than reported in the work detailed above [184]. Using PES and LEED, they reported that the initial deposition of Pt led to a disordered surface alloy. This model included a 1:1 ratio of Cu and Pt atoms in the surface layer, in agreement with the c(2×2) LEED pattern reported. As the coverage increased up to 2.0 ML, the alloy was destroyed and a disordered Pt film began to grow in a layer-by-layer fashion. Only annealing at temperatures of 300°C or above led to the reformation of the alloy. However, in contrast to the work of other groups described above, a pure Cu surface layer after annealing was not reported. Instead, a CuPt surface layer with a Cu_3Pt alloy in the next five layers was found. Obviously, a resolution to these conflicting reports must be found.

The objective of the work outlined in this chapter is to determine the true structural and compositional profile of the surface region during Pt deposition up to a coverage of $\sim$ 3 ML on the Cu(100) surface and to observe the changes which occur as a result of the subsequent annealing of the sample. CAICISS, LEED and XPS data were recorded at several Pt coverages to determine the relevant growth mode, with the ion scattering data being used to provide both a full structural fit and a layer-by-layer composition of the system at each deposition stage. Similar analysis has been carried out to study the structure and composition following a brief annealing of the sample.

6.2 Experimental details

The experiments were carried out on the Warwick modular CAICISS system, detailed in chapter 3. The Cu(100) crystal was aligned to an accuracy of $\pm$ 0.1° (verified by Laue measurements), spark eroded and mechanically polished prior to being loaded into the scattering chamber. Once loaded, the crystal underwent further *in-situ* cleaning by cycles of low energy IBA (3 keV Ar^+ for 30 minutes, followed by annealing at 800°C for 1 hour). The surface was deemed to be clean following the observation of a sharp (1×1) LEED pattern with low background intensity, in addition to negligible intensities in the O 1*s* and C 1*s* regions of the XPS spectrum. All XPS spectra were recorded using the Mg K_α anode ($h\nu$ = 1253.6 eV), with binding energies calibrated relative to the Cu $2p_{3/2}$ peak at 932.4 eV [142]. The analyser was operated in fixed analyser transmission (FAT) mode with a pass energy of 25 eV. Pt deposition was carried out using a metal evaporation source consisting of a high-purity Pt wire wound around a tungsten filament. To ensure that only Pt was being deposited from the source, the W 4*d* and 4*f* regions were monitored throughout the Pt deposition segments of the investigation, resulting in the knowledge that no W had been deposited on the surface. Resistive heating of the sample up to 800°C was monitored using a chromel-alumel thermocouple in contact with the sample. All CAICISS data were taken using a 3 keV He^+ ion beam with a step time of 100 s and a rotation of 1.8° between each step.

Scattering geometries

Figure 6.1(a) shows the scattering geometries in the <100> azimuth. Four distinct peaks can be expected, corresponding to scattering from the outermost five layers of the structure. In order of increasing polar angle, the first peak corresponds to scattering from atoms in the surface layer, whilst the second and third peaks arise from scattering in the second atomic layer of the structure. The fourth peak contains contributions from several different geometries, allowing the probing of the structure down to the fifth atomic layer.

Figure 6.1(b) shows the scattering geometries which contribute to the backscat-

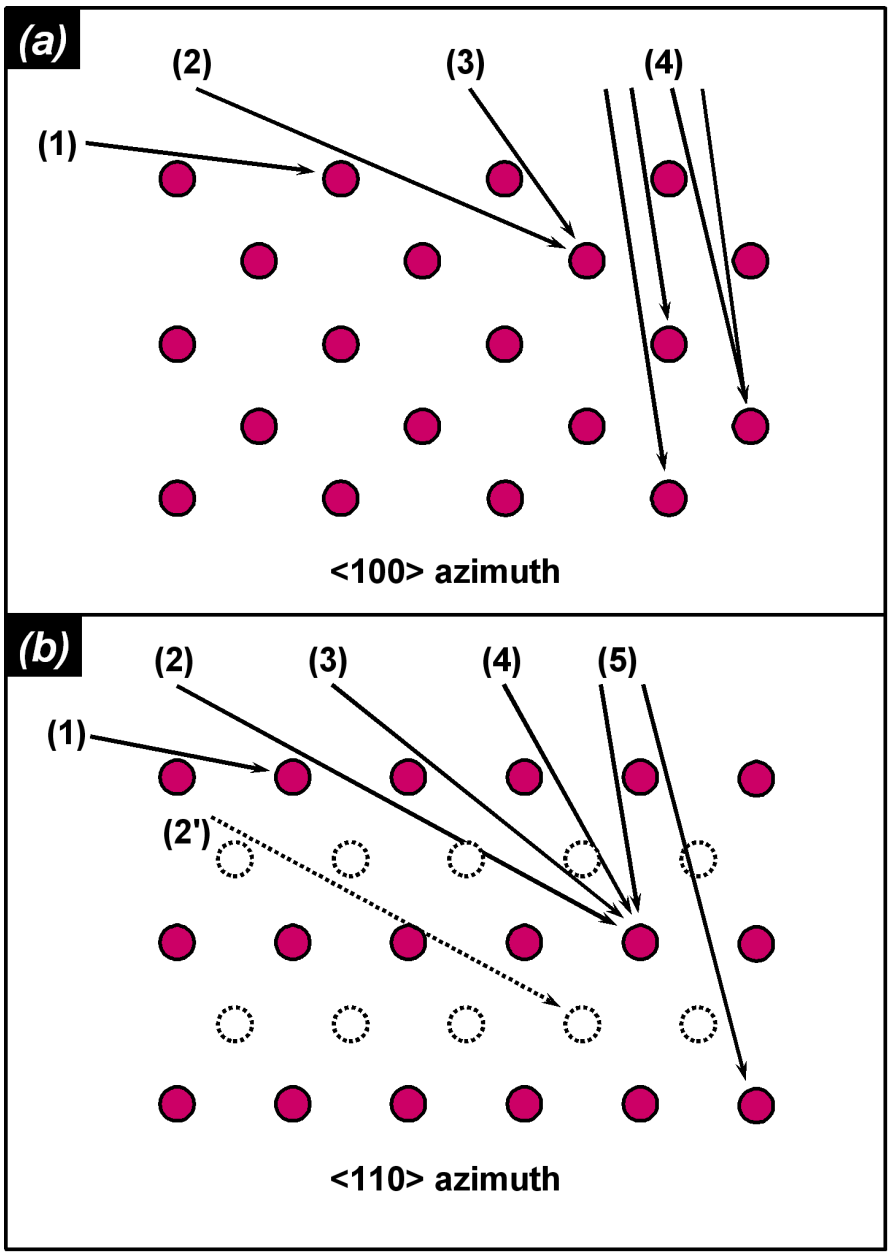

Figure 6.1: The scattering geometries which lead to peaks in the CAICISS spectra obtained in (a) the <100> and (b) the <110> azimuthal directions on the Cu(100) surface. This combination of azimuthal directions allows a full structural determination down to the fifth layer of the crystal. Atoms represented by dashed lines lie in different planes with respect to the incident ion beam.

tering spectrum produced by the Cu(100) structure with the ions incident in the <110> direction. Here, the distance between the first and third atomic layers can be probed in detail, in addition to the spacing between the second and fourth atomic layers (marked (2') in figure 6.1(b)). At near-normal incidence (direction 5), ions also penetrate to the fifth and sixth atomic layers of the structure.

Therefore, combination of the <110> and <100> azimuths offer the opportunity to probe the structure of the Cu(100) crystal down to the sixth atomic layer. Concentrations of Pt in these layers can also be determined from the CAICISS data taken following deposition.

6.3 Results

6.3.1 CAICISS study of the clean Cu(100) surface

Following the completion of the IBA process, a (1×1) LEED pattern was observed at 64 eV (shown in the inset of figure 6.2). Polar angle CAICISS spectra were then taken in both the <110> and <100> azimuths using the 3 keV He^+ ion beam. Plots of the Cu-backscattered intensity as a function of the time-of-flight (ToF) were then extracted using the method described in chapter 4.

Figure 6.2(a) shows the Cu-backscattered intensity as a function of the ToF extracted from the CAICISS data recorded in the <110> azimuth. The peak at 16° corresponds to the surface critical angle, at which one Cu surface layer atom focusses the incident ions on to the next surface layer atom in the <110> direction. Using the FAN software (figure 6.2(b)), it was found that a peak at this angle corresponds to an interatomic spacing of 2.56 ± 0.02 Å in the <110> direction and hence a lattice constant of 3.62 ± 0.02 Å [60]. Using this peak, it was also found that the correction factor to be applied to the screening length used in the Molière ion-atom interaction potential had to be approximately 0.53. This is in contrast to the expected value of ∼ 0.85 derived using equation 3.9 [90], and will be discussed further in the final chapter of this thesis.

The second, third and fourth peaks (at 29°, 45° and 66° respectively) in the

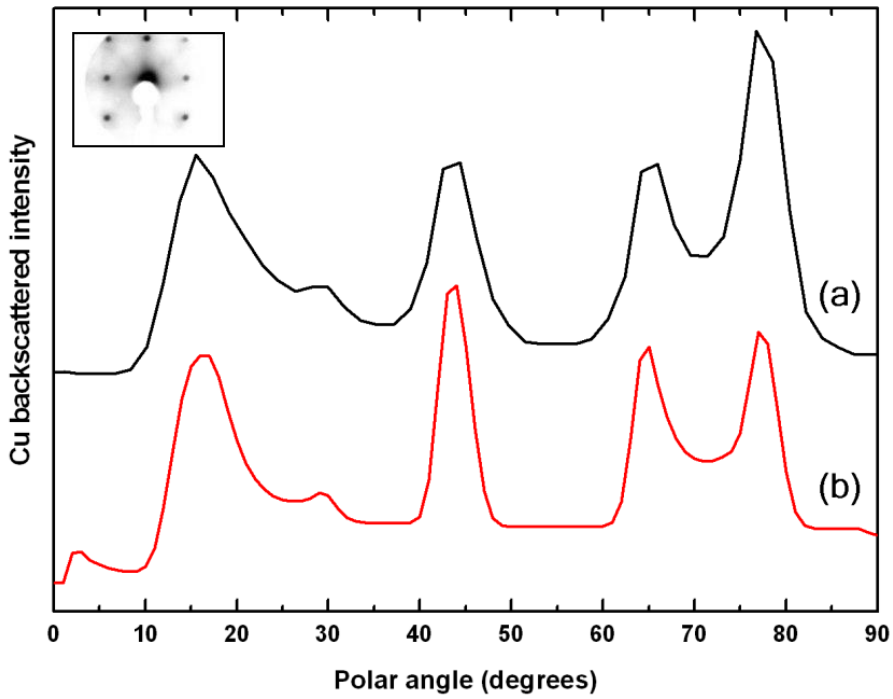

Figure 6.2: (a) CAICISS data from the clean Cu(100) surface in the <110> azimuth, along with (b) the simulated profile for the derived structure outlined in the main text. The inset in the upper-left shows the inverse of the (1×1) LEED pattern recorded at 64 eV prior to the CAICISS data being taken.

CAICISS data recorded in the <110> direction correspond to scattering from atoms in the third atomic layer (see figure 6.1(b)). These peaks also contain information on the distance between the second and fourth atomic layers (e.g. direction 2' in figure 6.1(b)). If the structure in the near-surface region is bulk-like, each peak would be described by a single component. However, relaxations in the near-surface region may necessitate a second component in order to fit each peak (i.e. the component arising from scattering by third-layer atoms will be at a slightly different angle to those arising from scattering from atoms in the fourth layer). Therefore, by careful consideration of the shapes of each of the peaks, it is possible to derive the spacing between each of the four outermost layers of the structure.

Using these features, the spacing between the first and third layers was found to be 3.57 ± 0.03 Å, whilst the second and fourth layers were found to be separated by

3.64 $\pm$ 0.03 Å. Careful consideration of the shape of each peak led to the adjustment of the distance between the first and second layers, Δ_{12}, until an acceptable fit was obtained on all peaks at a value of $\Delta_{12} = 1.74 \pm 0.02$ Å. This corresponds to a contraction of $\sim$ 4% on the bulk interlayer spacing of 1.81 Å. As a result of this finding, the distance between the second and third layers, Δ_{23}, was found to be 1.83 $\pm$ 0.02 Å, an expansion of $\sim$ 1.5% on the bulk interlayer spacing. Deeper layers were found to be separated by the bulk layer spacing of 1.81 Å.

Figure 6.3(a) shows the CAICISS data recorded in the <100> azimuth. Due to the larger interatomic spacing in the surface layer in this direction, the surface peak is found at a reduced angle of 12°. Analysis of this feature using the FAN software (figure 6.3(b)), using the same parameters as in the <110> case, led to the deduction of an interatomic spacing of 3.62 $\pm$ 0.03 Å in this direction, corresponding well with the known bulk interatomic spacing of 3.615 Å [60] and the value obtained from the data recorded in the <110> direction.

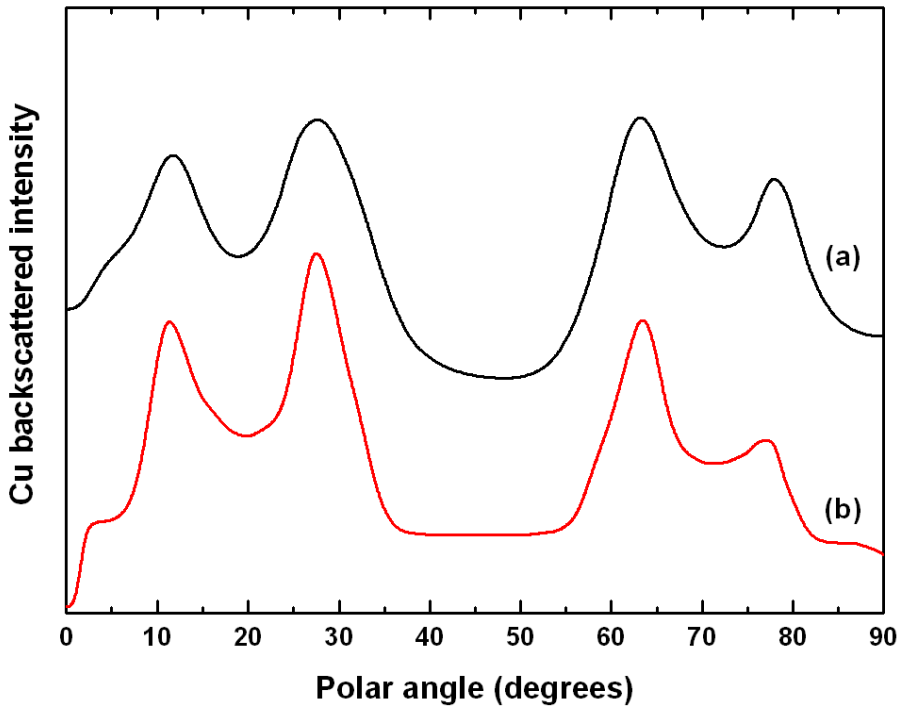

Figure 6.3: (a) CAICISS data from the clean Cu(100) surface in the <100> azimuth, along with (b) the simulated profile for the derived structure outlined in the main text.

The remaining peaks in the spectrum were used to establish the structure in the near-surface region. Analysis of the peaks centered at 28° and 62°, corresponding to scattering from atoms in the second layer, established Δ_{12} to be 1.75 $\pm$ 0.02 Å, a value in agreement with the spacing derived from the data recorded in the <110> direction. The final peak recorded was centered at 78° and was found to comprise components arising from scattering in the third, fourth and fifth layers of the structure. Analysis of this peak led to the conclusion that the structure was bulk-like when heading further into the structure from the third layer, in conjunction with an expansion of Δ_{23} to 1.83 $\pm$ 0.02 Å, again in agreement with the data obtained in the <110> azimuth.

In summary, the structure of the near-surface region was found to be only slightly different to the bulk Cu(100) structure. A contraction of $\sim$ 4% was found in the spacing between the first and second atomic layers, whilst an expansion of $\sim$ 1.5% was found in the distance between the second and third atomic layers. The structure of the crystal beyond the third atomic layer was found to be bulk-like, with an interlayer spacing of 1.81 Å. This model of the clean Cu(100) surface not only gives a good quantitative fit to CAICISS data in both azimuths, but also agrees with previously published data [12, 185].

Consideration of the results presented above shows that, within error, the same atomic structure for the clean Cu(100) surface region was derived in both the <110> and <100> azimuths. However, the peak at 78° in the <100> direction was found to comprise several components (see direction 4 in figure 6.1(a)). As shown in figure 6.1(b), the <110> azimuth offers the opportunity to probe the outermost five or six layers of the Cu(100) structure using several well-defined peaks which correspond to unique scattering geometries. Therefore all of the CAICISS data presented below were collected in the <110> azimuth as it enables a more accurate and efficient analysis of the structural and compositional profile of the surface region following the Pt depositions discussed in the following sections.

6.3.2 Initial growth of Pt on Cu(100)

With the structure of the clean Cu(100) surface determined, attention was turned to the characteristics of Pt deposition on the surface. This part of the investigation focussed on two themes - the growth mode of Pt on Cu(100) and any changes to the Cu(100) structure caused by the adsorption of Pt atoms. The results are summarized in table 6.1 (at the end of this section) and described in detail below.

The Pt backscattered intensity profile extracted from the CAICISS data recorded in the <110> azimuth following the deposition of 0.25 ML of Pt (determined by analysis of CAICISS and XPS data) is shown in figure 6.4. Also shown are FAN simulation profiles for three Pt growth models - layer-by-layer growth, 3D islands of

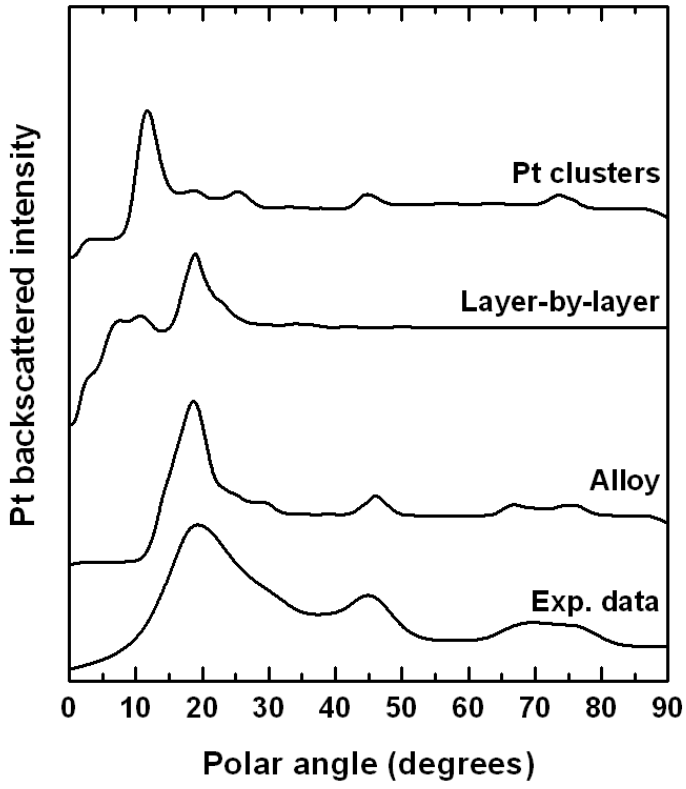

Figure 6.4: CAICISS data recorded in the <110> azimuth following the deposition of 0.25 ML of Pt on the Cu(100) surface. Also shown are the simulated profiles from three Pt growth models (layer-by-layer growth of a Pt film, 3D Pt-island formation and Cu-Pt alloy formation in the surface region). The features within the experimental data appears to favour the Cu-Pt alloy model.

Pt on the surface and an alloy in the surface and sub-surface regions. With no peak observed at $\sim 12^{\circ}$, the experimental data appear to rule out the formation of a Pt film on top of the surface, growing in either the Stranski-Krastanov or Frank-van der Merwe modes, both of which would commence with the formation of a complete Pt layer on top of the Cu(100) structure and are represented by the "layer-by-layer" profile in figure 6.4.

Consideration of the features of the experimental profile at higher polar angles leads to the exclusion of the Pt-islands model (ie. the Volmer-Weber growth mode). The extended alloy model is unique in predicting the features observed experimentally at 29° and 67°, peaks that correspond to scattering from Pt atoms in the third atomic layer of the Cu(100) structure. With these observations in mind, several trial structures were simulated using the FAN software to accurately determine the layer-by-layer composition of the alloy. The model structure yielding the best fit is shown in figure 6.4, with $18 \pm 1\%$ of the atoms in the surface layer found to be Pt atoms. Pt also made up $5 \pm 1\%$ of the second atomic layer and $2 \pm 1\%$ of the third atomic layer. Additionally, the two outermost interlayer spacings were observed to change to 1.95 ± 0.02 Å and 1.84 ± 0.02 Å, corresponding to expansions relative to the bulk Cu(100) structure of ~ 7.7 % and ~ 2.2 % respectively. Such expansions should be expected with the inclusion of larger Pt atoms into the Cu structure.

Considering the observation of a weak c(2×2) LEED pattern (inset of figure 6.5), the alloy formed during the deposition was not of uniform composition across the entire surface region. Most probably, the surface consisted of areas with a c(2×2) CuPt alloy structure, interspersed with purely Cu regions. This suggestion is reinforced by the broadness of the surface peak at 19° in the experimental CAICISS data, suggesting a range of interatomic distances in the surface layer. It can be expected that the Cu(100) structure could be significantly disrupted by the inclusion of larger Pt atoms into the lattice (a lattice mis-match of $\sim 8.5\%$). Indeed, the lattice mis-match, and hence the induced strain at the surface, may be the reason for the observation of Pt atoms in the sub-surface region as the surface tries to reduce its strain and hence energy by substituting Pt atoms into the sub-surface region. However, no Pt was

observed to penetrate to the fourth layer or deeper (including this in the simulations had a detrimental effect on the peak at 75°), with the interlayer spacings in this region remaining equal to the bulk Cu(100) value of 1.81 Å.

The broadness of the features within the experimental data when compared to the Cu-Pt alloy simulation in figure 6.4 suggests a small amount of distortion of the Cu(100) lattice in the regions around the Pt atoms which have been incorporated into the structure. Again, the lattice mis-match between the alloy constituents is the cause of this feature. The small differences in the shadow cones generated by Pt and Cu atoms in the surface layer will also be a contributing factor for the peaks arising from sub-surface Pt atoms.

The next step of the investigation commenced with a further Pt deposition, bringing the total Pt coverage to 0.55 ML. The CAICISS data recorded following the deposition is shown in figure 6.5. Once again, the layer-by-layer model can be discounted due to the observation of peaks at 45°, 68° and 78°, which must mean that not all of the Pt atoms reside in the same layer of the structure.

Comparing the remaining 3D Pt islands and Cu-Pt alloy models, it can be seen that all four peaks shown in the experimental profile in figure 6.5 are more accurately reproduced by the FAN simulation of the Cu-Pt alloy model. In this case, it was found that the top three layers contained Pt percentages of 45 $\pm$ 2%, 5 $\pm$ 1% and 5 $\pm$ 1%, with no Pt observed at greater depths.

Analysis of the experimental profile using the FAN software revealed that the outermost interlayer spacings had changed once again due to the inclusion of more Pt into the structure. Δ_{12} was found to be 2.00 $\pm$ 0.02 Å, a $\sim$ 10.5 % expansion relative to the bulk Cu(100) interlayer spacing and an expansion of $\sim$ 0.05 Å on the structure observed following the 0.25 ML Pt deposition. Δ_{23} was found to be 1.85 $\pm$ 0.02 Å, a $\sim$ 2.2 % expansion on the bulk spacing, but relatively close to the value deduced in the 0.25 ML Pt deposition case, indicating that most of the newly-deposited Pt was located in the surface layer. By correlation with the 0.25 ML Pt deposit, the spacings between the pure Cu layers deeper into the crystal were found to be, within experimental error, equal to the bulk Cu(100) value. Also correlating with the data

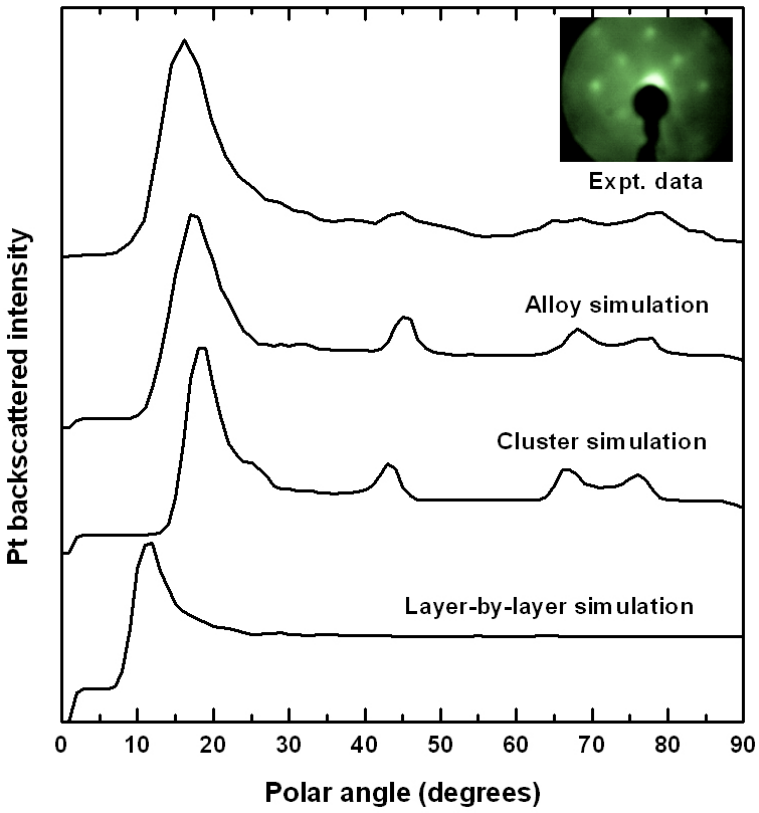

Figure 6.5: CAICISS data in the <110> azimuth following the deposition of 0.55 ML of Pt on the Cu(100) surface. Also shown are the simulated profiles from three Pt growth models, which predict that an alloy in the surface region has been formed. The inset in the upper-right shows the c(2×2) LEED pattern recorded at 130 eV from the surface.

recorded at a Pt coverage of 0.25 ML, the peaks detected at a 0.55 ML coverage seem to be broader than indicated in the simulated intensity profile. Again, this is most likely due to a small distortion of the Cu(100) structure around the Pt atoms, as well as the small differences in the shadow cones generated by Pt and Cu atoms in the surface layer.

Both sets of CAICISS data presented above show the existence of sub-surface Pt at sub-monolayer coverages. Small, but non-negligible amounts of Pt were observed to have penetrated beneath the surface. This is generally in agreement with the observations of Belkhou *et al.* who observed an alloy with a 1:1 compositional ratio in the surface layer [184] (close to the 45 % observed here), although they did not report

any sub-surface Pt. However, it would be very difficult to observe a small amount of sub-surface Pt using LEED and PES, whereas such features are easily seen in CAICISS experiments due to the existence of scattering geometries which exclusively probe the composition of the second and third layers of the structure.

Pt coverage (ML)	**0.00**	**0.25**	**0.55**	**1.00**	**2.35**	**2.75**	**300°C anneal**
LEED Pattern	(1×1)	weak c(2×2)	c(2×2)	streaky c(2×2)	none	none	weak c(2×2)
Overlayer (ML)	–	0	0	0	0.12	0.12	0.05
Layer 1 Pt %	–	18	45	80	87	100	50
Layer 2 Pt %	–	5	5	10	85	90	33
Layer 3 Pt %	–	2	5	10	50	55	25
Layer 4 Pt %	–	0	0	0	0	5	25
Layer 5 Pt %	–	0	0	0	0	15	25
Overlayer - surface (Å)	–	–	–	–	2.20	2.20	2.20
Δ_{12} (Å)	1.74	1.95	2.00	2.00	2.00	2.00	2.00
Δ_{23} (Å)	1.83	1.84	1.85	1.81	1.81	1.81	1.81
Δ_{34} (Å)	1.81	1.81	1.81	1.81	1.81	1.81	1.81
Δ_{45} (Å)	1.81	1.81	1.81	1.81	1.81	1.81	1.81

Table 6.1: LEED patterns, XPS data and results of FAN simulations of CAICISS data for Pt deposition up to 2.75 ML and subsequent annealing at 300°C. The data show the existence of Pt in the sub-surface region at sub-monolayer Pt coverages, discounting the previously proposed models which suggested the formation of Pt islands on the surface. The inclusion of Pt atoms into the Cu(100) lattice leads to the expansion of the interlayer spacings near the surface. Following annealing, significant amounts of Pt diffuse into the bulk Cu(100) structure. The total Pt coverages determined by XPS are accurate to $\pm$ 0.05 ML. The individual layer compositions were determined by CAICISS and are accurate to $\pm$ 5%. The interlayer spacings, determined by CAICISS, are accurate to $\pm$ 0.02 Å.

6.3.3 Deposition of Pt up to a $\sim$ 3 ML coverage

The second part of the investigation was to observe the growth characteristics as the total Pt coverage was increased up to $\sim$ 3 ML, in analogy to the studies of Belkhou *et al.*, which looked at the results of a 2.0 ML Pt deposition [184]. CAICISS experiments were performed on surfaces with Pt coverages of 1.00, 2.35 and 2.75 ML, with the Pt deposited at room temperature (all coverages accurate to $\pm$ 0.05 ML). As the coverage increased, the c(2$\times$2) LEED pattern (previously shown in figure 6.5) became progressively weaker with an increasing background intensity. No LEED spots were visible at or above a Pt coverage of 2.35 ML, suggesting the formation of a disordered structure at the surface.

The Pt-backscattered intensity profile extracted from the CAICISS data recorded in the <110> azimuth following each deposition stage is shown in figure 6.6. The plots firstly show an increase in the intensity of the surface peak ($\sim$ 16°) between the 0.55 ML and 1.00 ML cases. However, the other peaks, which correspond to scattering from sub-surface Pt atoms, showed only a small increase in intensity, indicating that just a small proportion of the newly-deposited Pt had penetrated below the surface layer. FAN simulation results (detailed in table 6.1) indicated that the observed change in the intensity of the surface peak was due to an increase in the surface Pt concentration to 80 $\pm$ 4%. The results also indicated that the Pt concentration in the second and third layers had both increased to 10 $\pm$ 1% as a result of increasing the total Pt coverage to 1.00 $\pm$ 0.05 ML.

With the surface layer now consisting of mostly Pt, a further deposition was implemented to investigate whether the additional Pt would form a film on top of the surface, or alternatively form a sub-surface alloy. Analysis of the data taken at a coverage of 2.35 $\pm$ 0.05 ML shows a dramatic increase in the Pt concentration in the second a third atomic layers, as evidenced by the increase in the intensity of the features at polar angles in excess of 40°. Analysis of these features using the FAN software revealed Pt concentrations of 87 $\pm$ 4% in the surface layer, 85 $\pm$ 4% in the second layer and 50 $\pm$ 3% in the third layer of the structure. Again, no Pt was thought to have penetrated into the fourth layer of the structure or below. However,

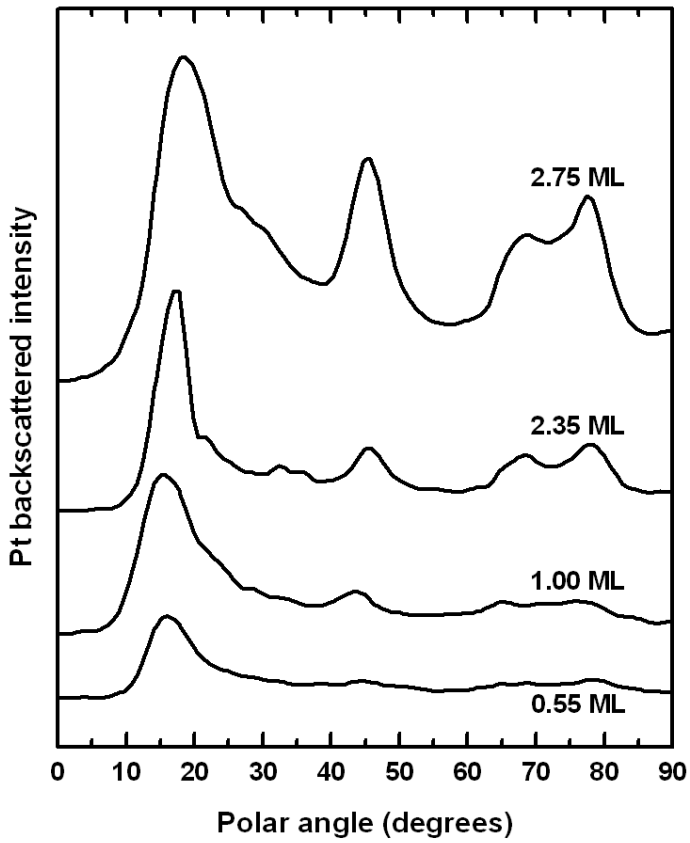

Figure 6.6: CAICISS Pt peak profile as a function of Pt coverage. Peaks corresponding to sub-surface Pt are present at sub-monolayer coverage suggesting the formation of an alloy on deposition. These peaks increase in intensity with further Pt deposition up to 2.75 ML.

a small number of Cu atoms are still able to diffuse to the surface. This is most likely in an effort to lower the surface energy of the system as Cu has a lower surface energy that Pt [60].

Interestingly, the structure of the near-surface region at a Pt coverage of 2.35 ML was found to be similar to the structure derived from the experiments performed at a Pt coverage of 1.00 ML. The most likely scenario is that there was a small increase in the interlayer spacings ($\sim$ 0.01 Å), but that the increase is within the experimental error. The mean radii of the shadow cones arising from atoms in the surface layer also increases as more Pt atoms are included into the surface layer, meaning that features corresponding from sub-surface scattering events would appear at higher polar angles.

These factors would account for the small increase of the polar angle with increasing Pt coverage, as shown in figure 6.6.

A partial Pt overlayer (0.12 $\pm$ 0.02 ML), 2.20 $\pm$ 0.03 Å above the surface layer was required to reproduce the feature observed at 32° at coverages of 2.35 and 2.75 ML. This observation suggests the onset of the growth of a disordered Pt film, growing in a layer-by-layer fashion, and is a further reason for the slight increase in the polar angles of the features arising from sub-surface scattering. In the case of an overlayer, it is possible to observe features arising from ions being focussed from atoms in the overlayer on to atoms in the first complete (surface) layer. As the 2.20 Å 'gap' to the overlayer is larger than Δ_{12} (2.00 Å), some broadening of the features at higher polar angles should be expected.

Increasing the Pt coverage to 2.75 ML also saw the formation of a pure Pt surface layer, augmenting the evidence for the onset of thin film growth at Pt coverages above $\sim$ 2 ML. The Pt concentrations in the second and third layers increased slightly (to 90 $\pm$ 4% and 55 $\pm$ 3% respectively), whilst small amounts of Pt were observed for the first time in the fourth and fifth layers (5 $\pm$ 3% and 15 $\pm$ 3% respectively). Again, no distinguishable changes to the structure in the surface region were observed as a result of the extra Pt deposition.

Figure 6.7 shows the evolution of the Cu 3*p* and Pt 4*f* peaks as a function of Pt coverage, with all data recorded at a take-off angle of 45°. The intensity of the Cu $3p_{1/2}$ peak is observed to decrease relative to the Pt 4*f* peaks, with only a small shoulder corresponding to the Cu $3p_{1/2}$ peak, centered at $\sim$ 77 eV, visible at Pt coverages in excess of $\sim$ 1 ML. These data add weight to the argument that a Pt-rich surface has been formed and that there are only a small number of Cu atoms in the outermost two layers at Pt coverages in excess of $\sim$ 2 ML. It should be noted that these data were also used to obtain an estimate of the amount of Pt deposited using the equations detailed in section 3.4, and therefore acted as a starting point for the simulations of the CAICISS data using the FAN software.

Whilst data at higher Pt coverages were not recorded, the CAICISS data presented above suggests that further Pt deposition would lead to the formation of a pure Pt

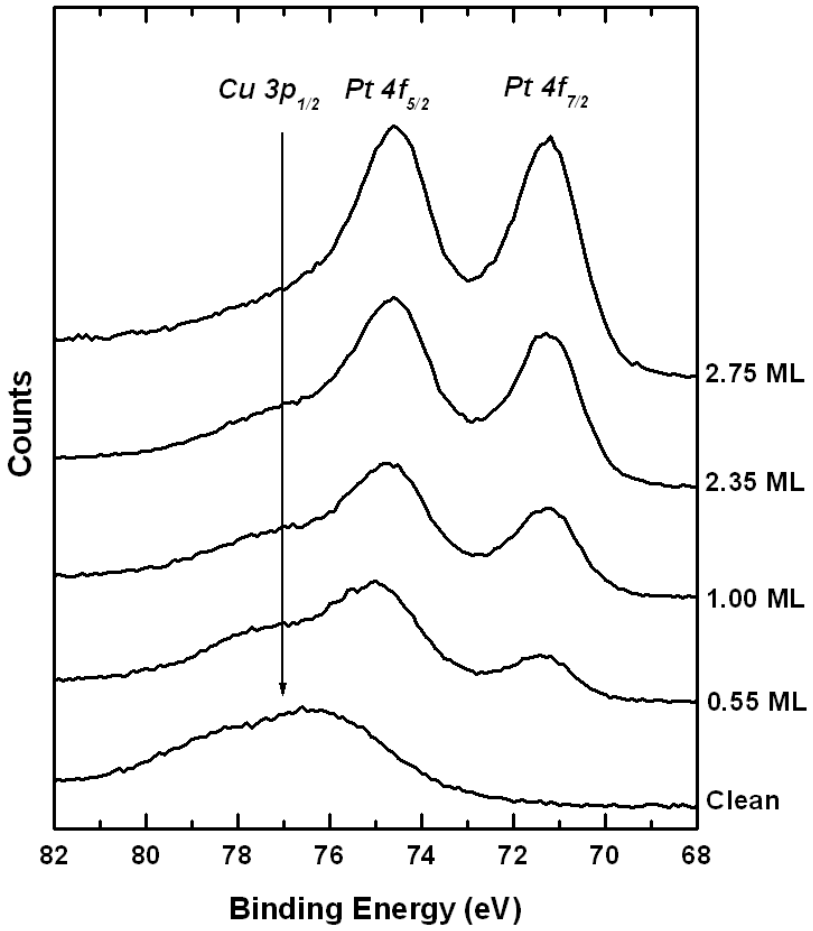

Figure 6.7: The Pt 4f (71.2 eV, 74.5 eV) and Cu 3p (75.2 eV, 77.5 eV) photoemission peaks from clean Cu(100) and during Pt deposition up to a coverage of 2.75 ML. All data were recorded at a take-off angle of 45°.

film of several monolayers in thickness on the surface. The expansion in the interlayer spacings at the surface (table 6.1) lends support to this argument, given that the interatomic spacing in Pt films (3.924 Å) is 8.5 % larger than in the Cu structure (3.615 Å). This difference corresponds reasonably well with the 10.5 % expansion in the topmost interlayer spacing observed during this investigation. Therefore, the structure at the surface is tending towards the f.c.c. Pt(100) structure. However, the Pt film would most likely still be disordered at the higher Pt coverages and requires a brief annealing treatment to restore an ordered structure.

6.3.4 Annealing of Pt films on Cu(100)

The final part of this investigation focussed on the effects on the structure and composition of the surface region as a result of annealing the sample with a Pt coverage of 2.75 ML. Firstly, the sample was annealed at 200°C, yielding no discernable change in the Pt backscattered profile from CAICISS and no obvious features in the LEED pattern. These observations are in agreement with previous work on this metal-metal system, which has suggested that Pt begins to diffuse into the Cu substrate at temperatures in excess of 230°C [183, 184].

Figure 6.8 shows the Pt backscattered profile extracted from the CAICISS data which was recorded both before and after annealing to 300°C for 10 minutes, along with the corresponding LEED patterns which were observed. As the insets of figure 6.8 demonstrate, a weak c(2×2) LEED pattern was observed following annealing, suggesting that some ordering had occurred in the surface region. The features contained within the CAICISS data also appear to be a little more sharply defined following annealing, again suggesting that some ordering has occurred within the structure.

The two sets of CAICISS data presented in figure 6.8 have been normalised such that the intensities of the surface peaks in the two profiles are identical. This approach shows the increase in the backscattered yield at 45°, 65° and 77°, which correspond to scattering from sub-surface atoms. From FAN simulations, it was found that a significant amount of Pt had diffused into the Cu substrate (see table 6.1). The partial Pt overlayer had been reduced to 0.05 ± 0.01 ML from a coverage of 0.12 ± 0.01 ML prior to annealing. In addition, a CuPt alloy layer with a 1:1 compositional ratio was found at the surface. Below this, a second layer with an average Cu_2Pt composition was found, whilst the composition of the other layers within the probing depth of the CAICISS experiment ($\sim$ 5 layers) was found to be Cu_3Pt. However, no purely Cu layers were observed in the structure, in contrast to the observations of Al Shamaileh *et al.* [182] and Reilly *et al.* [183]. Indeed, the observations presented here support the work published by Belkhou *et al.*, where a CuPt surface layer and a Cu_3Pt sub-surface alloy were reported [184].

Finally, figure 6.9 shows the Pt 4*f* and Cu 3*p* region of the XPS spectra taken at

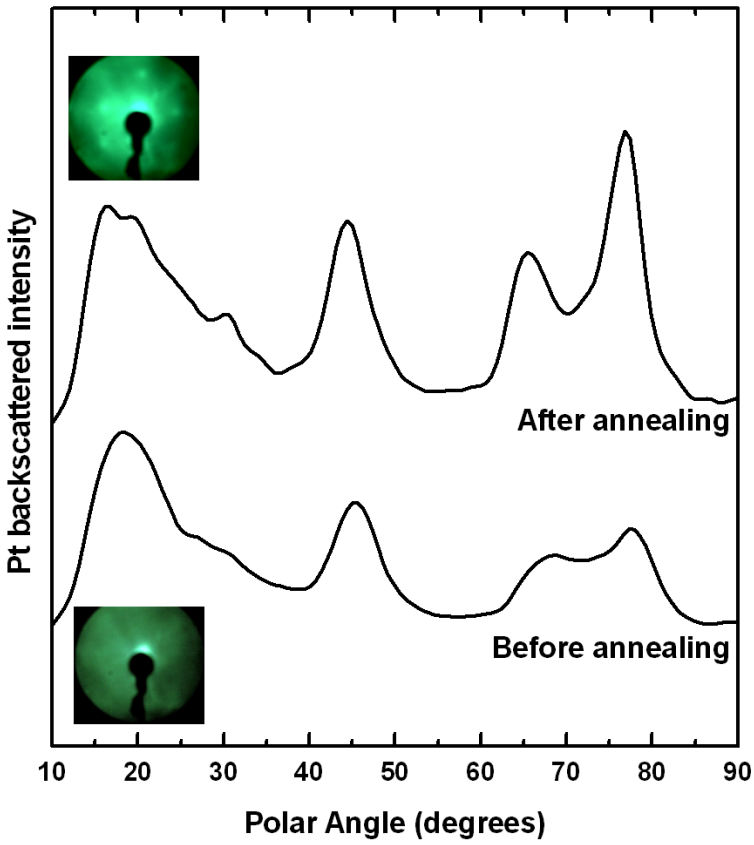

Figure 6.8: CAICISS and LEED observations from the surface with a Pt coverage of 2.75 ML prior to and following annealing at 300°C for 10 minutes. Both CAICISS and LEED show signs of some ordering at the surface caused by the annealing treatment. The increase of the intensities of the features at higher polar angles suggests that a significant proportion of the Pt at the surface has diffused into the sub-surface region during annealing. Both LEED patterns shown were recorded at 130 eV.

three different points of this investigation. The clean spectrum shows the position of the Cu 3*p* peaks, centered at approximately 76 eV. The broadness of this feature is due to the low intensity of the peak and the small separation of the $3p_{1/2}$ (77.5 eV) and $3p_{3/2}$ (75.2 eV) components. Depositing 2.75 ML of Pt on the surface led to the complete loss of the Cu 3*p* peaks from the spectrum, indicating that the outermost few layers were almost entirely composed of Pt atoms. The Pt $4f_{7/2}$ and $4f_{5/2}$ peaks were recorded at 71.0 and 74.2 eV respectively, roughly in line with values obtained from bulk Pt (shown in chapter 6). The Cu 3*p* features were only recovered upon annealing the sample to 300°C, illustrating that some Cu atoms had diffused back

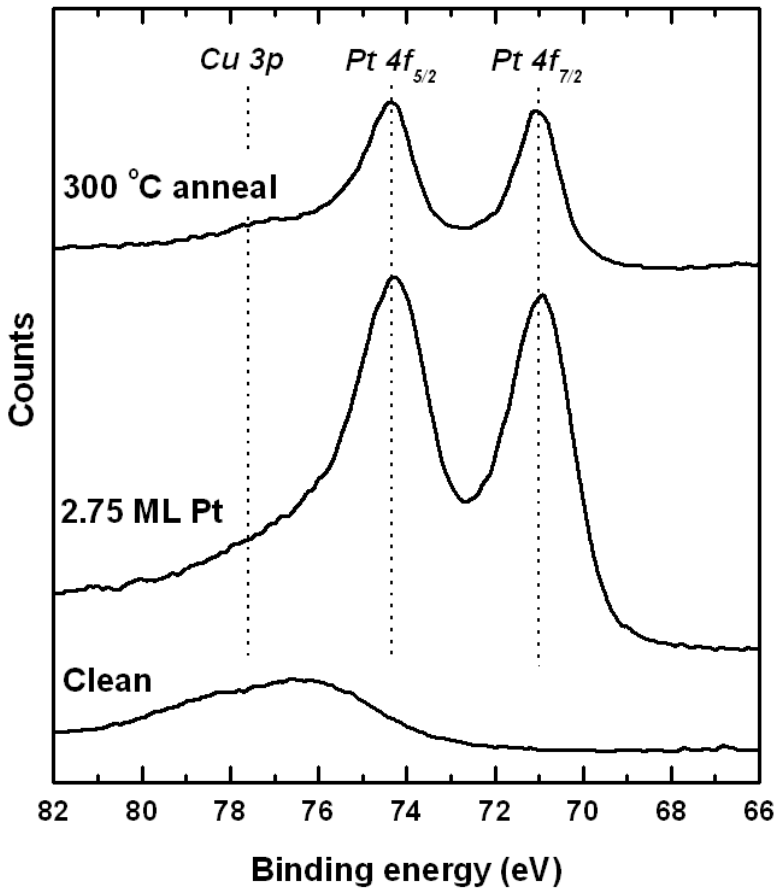

Figure 6.9: The Pt 4*f* and Cu 3*p* region of the XPS spectra taken from the surface at three stages of the investigation. The clean surface shows only the Mg K_α Cu 3*p* peaks. At a Pt coverage of 2.75 ML, only the Pt 4*f* peaks were observed, with the Cu 3*p* peaks re-emerging following annealing at 300°C.

to the surface layer, hence showing the formation of an extended Pt-Cu alloy in the outermost layers of the structure.

6.4 Conclusions

The structure and composition of Pt films and alloys formed on the Cu(100) surface has been investigated. Firstly, a (1×1) LEED pattern was observed and the structure of the clean Cu(100) surface then investigated using CAICISS. The ion scattering results showed a small contraction in the outermost interlayer spacing of ~ 4

%. An expansion of ~ 1.5 %, was observed in the second interlayer spacing, with layers deeper in the crystal separated by the bulk spacing of 1.81 Å. These observations were found to be in general agreement with previous studies [12, 185], and best described the CAICISS data recorded in both the <100> and <110> azimuths. However, the analysis of both data sets required the use of a correction factor to the Firsov screening length of 0.53, a very low value when compared to the 0.85 predicted using the work of O'Connor *et al.* [90]. This topic will be discussed further in the final chapter of this thesis.

The initial structures formed by depositing Pt on the Cu(100) surface were also studied using CAICISS and LEED. A weak c(2×2) LEED pattern indicated a disordered alloy surface. CAICISS data proved the existence of sub-surface Pt atoms at coverages of 0.25 ML and 0.55 ML, discounting previous models which claimed the formation of Pt islands on the surface [181, 182]. CAICISS data also showed an expansion in the two outermost interlayer spacings due to the inclusion of Pt into the Cu structure with, in the 0.55 ML case, $\Delta_{12} \sim 7.7$ % larger than the bulk Cu(100) interlayer spacing, whilst Δ_{23} was ~ 2.2 % larger. In both the 0.25 ML and 0.55 ML case, the majority of the Pt was found to reside in the surface layer.

The build-up of Pt in the surface region continued with a further deposition stage, bringing the total coverage up to 1.0 ML. At this stage, Pt atoms constituted 80% of the surface layer and 10 % of both of the second and third layers of the structure.

As the Pt deposition continued, the c(2×2) LEED pattern became obscured by an increasing background intensity. No diffraction spots were distinguishable at coverages of 2.35 ML and 2.75 ML, indicating significant disorder at the surface. Analysis of the CAICISS data recorded at a coverage of 2.75 ML revealed the existence of a partial Pt overlayer on top of a purely Pt surface layer. The majority of the constituents of the second and third layers were also found to be Pt atoms, with the Pt-rich surface region suggesting the onset of the growth of a disordered Pt film. XPS spectra revealed an almost complete loss of Cu from the surface region at a coverage of 2.75 ML, supporting the notion that the outermost few layers were composed almost entirely of Pt atoms. Hence, CAICISS and XPS spectra both indicate the onset of the

layer-by-layer growth of a Pt film at (and in excess of) the coverages studied.

Annealing of the sample with a Pt coverage of 2.75 ML at 300°C for 10 minutes yielded the restoration of a weak c(2×2) LEED pattern. This suggests that some ordering occurs in the surface region, an observation reinforced by the sharpening of the features in the CAICISS profile recorded after annealing. The CAICISS data also revealed significant diffusion of Pt into the bulk at this temperature, correlating well with previous studies. However, no pure Cu layers were observed which is in contrast to some of the studies previously published on this system. Instead, a CuPt surface alloy layer was found, with a Cu_2Pt layer below it and the third to fifth layers of Cu_3Pt composition. This is roughly in line with the findings of Belkhou *et al* [184]. However, the work presented here adds to the previous findings, with the CAICISS data giving compositional and structural information at several different Pt coverages and, following the annealing of the sample, shows that Pt penetrates into the sub-surface region at sub-monolayer coverages.